Apolipoprotein O is mitochondrial and promotes lipotoxicity in heart

Annie Turkieh,[1] Céline Caubère,[1] Manon Barutaut,[1] Franck Desmoulin,[1] Romain Harmancey,[1] Michel Galinier,[1,2] Matthieu Berry,[1,2] Camille Dambrin,[2] Carlo Polidori,[3] Louis Casteilla,[4] François Koukoui,[1] Philippe Rouet,[1] and Fatima Smih[1]

[1]INSERM U1048 Equipe no. 7, Obésité et insuffisance cardiaque: approches moléculaires et cliniques, Toulouse, France. [2]Hôpital Rangueil, Toulouse, France. [3]University of Camerino, Camerino, Italy. [4]INSERM U1031 Equipe no. 1, Toulouse, France.

Diabetic cardiomyopathy is a secondary complication of diabetes with an unclear etiology. Based on a functional genomic evaluation of obesity-associated cardiac gene expression, we previously identified and cloned the gene encoding apolipoprotein O (APOO), which is overexpressed in hearts from diabetic patients. Here, we generated APOO-Tg mice, transgenic mouse lines that expresses physiological levels of human APOO in heart tissue. APOO-Tg mice fed a high-fat diet exhibited depressed ventricular function with reduced fractional shortening and ejection fraction, and myocardial sections from APOO-Tg mice revealed mitochondrial degenerative changes. In vivo fluorescent labeling and subcellular fractionation revealed that APOO localizes with mitochondria. Furthermore, APOO enhanced mitochondrial uncoupling and respiration, both of which were reduced by deletion of the N-terminus and by targeted knockdown of APOO. Consequently, fatty acid metabolism and ROS production were enhanced, leading to increased AMPK phosphorylation and *Ppara* and *Pgc1a* expression. Finally, we demonstrated that the APOO-induced cascade of events generates a mitochondrial metabolic sink whereby accumulation of lipotoxic byproducts leads to lipoapoptosis, loss of cardiac cells, and cardiomyopathy, mimicking the diabetic heart–associated metabolic phenotypes. Our data suggest that APOO represents a link between impaired mitochondrial function and cardiomyopathy onset, and targeting APOO-dependent metabolic remodeling has potential as a strategy to adjust heart metabolism and protect the myocardium from impaired contractility.

Introduction

Increased susceptibility to cardiac injury in obesity and diabetes is evident in both human and animal studies (1–4). Cardiovascular complications are the leading cause of diabetes-related morbidity and mortality. Obesity and diabetes are well-known causes of heart failure, and their prevalence continues to increase markedly. Indeed, the number of current and expected patients with diabetes will translate into extremely high healthcare costs. Diabetic cardiomyopathy, a progressive disease, describes the changes in cardiac structure and function secondary to diabetes, in the absence of hypertension or vascular pathology (5). Diabetic cardiomyopathy is characterized by a myriad of functional and structural alterations of the heart, such as echocardiographic changes consistent with systolic dysfunction, cardiac metabolic switch for increased fat consumption, lipotoxicity, and enhanced oxidative stress (2, 3). In light of these many contributory functional abnormalities, it remains unclear which factors are primary and of causal importance to the development of diabetic cardiomyopathy.

Through a functional genomics study aimed at identifying genes differentially regulated in the heart by obesity, we discovered apolipoprotein O (APOO), which is overexpressed in hearts from diabetic patients (6) and in animal hearts after 9 weeks of high-fat diet (HFD) feeding, i.e., in the early phases of metabolic stress (7). APOO's 198-aa-long peptide sequence is conserved from unicellular eukaryotes to humans. Sequence analysis revealed a slightly negatively charged N-terminus and a medium overall hydrophobicity. APOO possesses a homologous apolipoprotein A1, A-IV, and E family domain sequence and was detected in the bloodstream, where it was mainly present on high-density lipoproteins (6). In yeast and *C. elegans*, *Apoo* orthologs are located within the inner mitochondrial membrane in hetero-oligomeric protein complexes termed mitochondrial inner membrane organizing systems (MitOS) (8, 9). MitOS components are involved in the maintenance of the characteristic morphology of the inner mitochondrial membrane and the connection between inner boundary and cristae membranes. In the present work, we showed that at least one protein from this complex, APOO, unpredictably played a more active role than structural organizer. Apolipoproteins were first identified to bind lipoproteins that facilitate plasma lipid transport through the lymphatic and circulatory systems. However, additional unexpected functions have also been identified for apolipoproteins: APOE activates Akt/PKB phosphorylation (10); APOJ can be translocated to the nucleus, where it binds to DNA repair protein Ku80 (11); and APOL6, which has structural homologies with BCL-2 family members, regulates pathways such as autophagy (12).

In order to uncover how changes in APOO expression relate to modifications of cardiac function, we performed in silico, in vitro, and in vivo manipulations using (a) cardiac myoblasts, (b) 3 independent cardiac-specific transgenic mouse lines expressing APOO at physiological levels (referred to herein as APOO-Tg mice), (c) in vivo transfected mouse liver, and (d) human heart samples. We showed that APOO localizes to mitochondria in cardiomyocytes and enhances uncoupling. This leads to a specific cascade of maladaptive events leading to cardiomyopathy. We demonstrated the

Authorship note: Annie Turkieh and Céline Caubère contributed equally to this work.

Conflict of interest: The authors have declared that no conflict of interest exists.

Citation for this article: *J Clin Invest.* 2014;124(5):2277–2286. doi:10.1172/JCI74668.

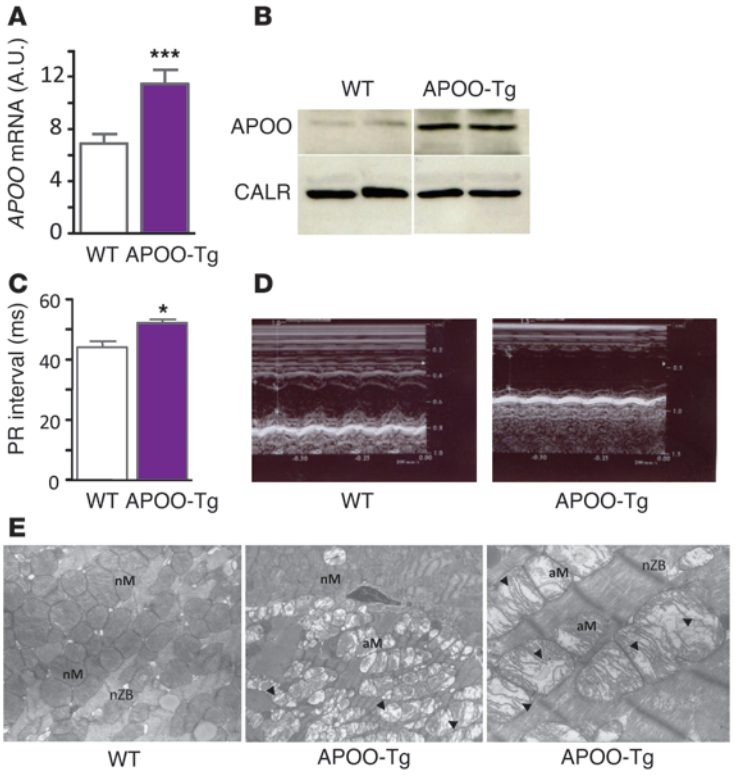

Figure 1

Characterization of APOO-Tg mice. (**A**) *APOO* mRNA levels in WT (n = 38) and APOO-Tg (n = 32) mice. (**B**) APOO (55 kDa) Western blot analysis of WT and APOO-Tg mouse heart extracts. Calreticulin (48 kDa) was used as loading control and detected with calreticulin antibody on the same membrane after dehybridization. Lanes were run on the same gel but were noncontiguous. (**C**–**E**) WT and APOO-Tg mice were aged 18–20 weeks and fed HFD for 9–10 weeks. (**C**) PR interval, measured from the beginning of the P wave to the beginning of the QRS complex. (**D**) Representative echocardiographic images. (**E**) TEM of myocardial sections (longitudinal). Arrowheads denote cristae in markedly altered mitochondria (aM). nM, normal mitochondria; nZB, normal Z bands. Original magnification, ×10,000 (left and center), ×15,000 (right). *P < 0.05, ***P < 0.001. Data represent mean ± SEM.

importance of APOO as a new signal regulator of mitochondrial function and cardiac metabolism. The APOO model represents an original link between impaired mitochondrial function and the onset of cardiomyopathy. Our present findings outline the interplay between mitochondrial dysfunction and lipotoxicity.

Results

APOO is mitochondrial and associates with heart dysfunction in mice and humans. Examination of publicly available human heart microarray datasets (from patients undergoing cardiac transplantation and from "normal" organ donors; see Methods) revealed that *APOO* mRNA levels fluctuated between 1 and 5 AU. Pathway analysis using synthetic expression ratios between microarrays with the highest and lowest *APOO* expression revealed enrichment in various metabolic pathways, the most significant being oxidative phosphorylation and mitochondrial dysfunction (Supplemental Figure 1, A–D; supplemental material available online with this article; doi:10.1172/JCI74668DS1). We generated transgenic mouse lines constitutively expressing human APOO in heart at physiological levels (<3-fold endogenous APOO; Figure 1, A and B). Under a HFD, the APOO-Tg mice exhibited depressed ventricular function. Specifically, these mice displayed a lengthening of the PR interval and reductions in ejection fraction (56.65% ± 1.74% vs. 63.41% ± 2.11%, P < 0.05), fractional shortening (25.45% ± 1.08% vs. 29.77% ± 1.320%, P < 0.05), and LV posterior wall thickness (48.47% ± 4.70% vs. 65.05% ± 3.89%, P < 0.05) (Figure 1, C and D). Transmission electron microscopy (TEM) analysis of longitudinal myocardial sections revealed mitochondrial degenerative changes, such as loss or discontinuity of cristae and swelling (Figure 1E and Supplemental Figure 2A). Irreversible disorganization and degeneration in the myocardium, like myofibrillar disarray and decreased myofibrillar content, were evident. In some cardiomyocytes, a widening of intercellular junctions was also observed. In severely affected areas, we observed intercellular dissociation and ultrastructural evidence of marked loss of contractile elements, which produced a diffuse pattern in defective myocytes that led to cell death (Supplemental Figure 2, B–E), correlating with the alteration of hemodynamic parameters. In silico investigation of the APOO sequence revealed a putative N-terminal mitochondrial "address label." We then designed expression vectors and generated different cardiac myoblast transfectants expressing human APOO (referred to herein as APOO cells), as well as APOO cells in which *APOO* expression was diminished by transfection of *APOO* shRNA vectors (sh*APOO*; Supplemental Figure 3, A–C) and APOO cells with N-terminal deletion of 40 aa of APOO. In vivo fluorescent labeling, as well as studies with protein extracts and subcellular fractions from APOO cells, revealed a mitochondrial localization for this protein (Figure 2, A–C). Deletion of the 40 N-terminal residues changed APOO distribution from the mitochondria to the cytoplasm (Figure 2, D and E). Furthermore, hydrodynamics-based in vivo mouse liver transfection by rapid tail vein injection of pTT-APOO expression vector led to a rise in *APOO* expression, as evidenced by PCR amplification of the transfected expression vector and an increased level of APOO protein in the mitochondria (Supplemental Figure 4, A–C).

APOO promotes mitochondrial uncoupling and respiration. APOO cells displayed a 2-fold increase in basal oxygen consumption that was dependent on mitochondrial localization of APOO and ablated by sh*APOO* treatment (Figure 3A). Antimycin, an inhibitor of the quinone cycle, almost completely inhibited oxygen consumption (Figure 3B), which indicates that most of the respiration being measured is mitochondrial. Basal oxygen consumption was partly inhibited by oligomycin in APOO cells, and addition of the uncoupler carbonyl cyanide m-chlorophenyl hydrazone led to a 2-fold increase in oxygen consumption (Figure 3B), which suggests that these cells have enhanced electron transport activity. Respiration coupling (RC) calculations revealed decreased RC in APOO cells (Figure 3C). We observed equivalent results with isolated mitochondria from hydrodynamics-based in vivo transfected mouse liver, which displayed a significant increase in oxygen consumption (Supplemental Figure 4D). These effects were also associated with increased intracellular ROS (Figure 3D). Thus, APOO has 2 distinct effects on mitochondrial function: an increase in uncoupling and an increase in total respiration.

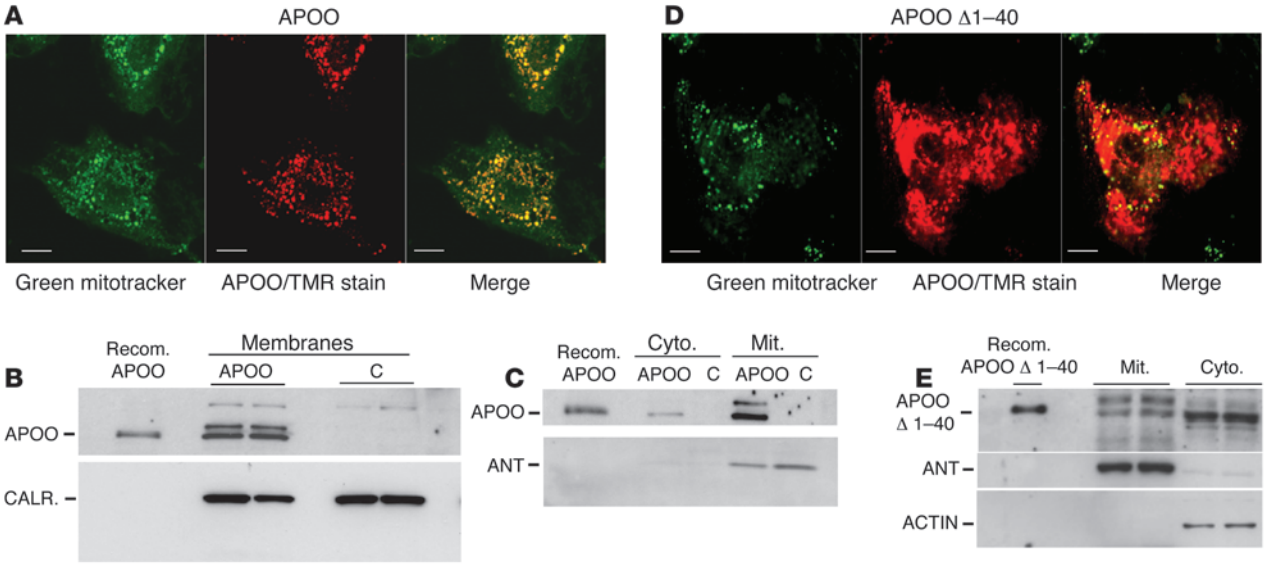

Figure 2

In vitro analysis of APOO in cardiac myoblasts. (**A**) Confocal microscopy of H9c2 cardiac myoblasts transfected with SNAP-tagged hAPOO. (**B**) Western blot for APOO (55 kDa) with membrane protein extracts prepared from APOO and control (C) cells. Equal lane loading and transfer were verified by probing the same membrane with calreticulin (CALR, 48 kDa) antibody. (**C**) Western blot analysis of cytoplasmic and mitochondrial fractions of control cells and cardiac myoblasts overexpressing APOO hybridized with APOO antibody. Mit, mitochondria; Cyto, cytoplasm. (**D**) Confocal microscopy of H9c2 cardiac myoblasts transfected with SNAP-tagged N-terminal deletion of 40 aa of APOO (APOO Δ1–40). (**E**) Western blot analysis of cytoplasmic and mitochondrial fractions of control cells and cardiac myoblasts overexpressing APOO Δ1–40 hybridized with APOO antibody. Recombinant (Recom) proteins were used for size control. Actin (42 kDa) and ANT (33 kDa) were used as cytosolic and mitochondrial purification controls, respectively. Mitochondria were stained with green mitotracker; SNAP-APOO and SNAP-APOO Δ1–40 were revealed with TMR-star. Shown are representative data from 1 experiment. Experiments were repeated 3 times. Scale bars: 10 μm.

We observed a significant increase in cytochrome C oxidase activity, a mandatory component of the respiratory chain, in APOO cells and APOO-Tg hearts (Figure 3E and Supplemental Figure 5). We also demonstrated a significant increase in the expression of oxidative phosphorylation genes in APOO cells, which was reduced by both N-terminal deletion of APOO and sh*APOO* treatment (Figure 3, F and G).

APOO enhances fatty acid metabolism. *APOO* is highly expressed in mitochondria-enriched tissues that mainly use fatty acids as an energy source (6). Therefore, we assumed that the APOO-induced increase in electron transport chain flux would increase the mitochondrial use of long-chain fatty acids (LCFAs) and induce a mitochondrial metabolic sink. Indeed, in order to provide mitochondria with LCFAs, cells would ultimately increase fatty acid uptake at the plasma membrane.

We analyzed whether APOO could induce the expression of genes involved in fatty acid metabolism. Long-chain acyl-CoA synthetase (ACSL) and FATP4 catalyze LCFA esterification, allowing lipid channeling. In APOO cells, fatty acid transporter (CD36 and FATP4) expression and ACSL activity were strongly increased, effects that were significantly reversed by treatment with either sh*APOO* or the ACSL inhibitor triacsin C (Figure 4, A–C). Accordingly, we measured rapid accumulation of green fluorescent BODIPY-palmitate in APOO-expressing cells and found that basal intracellular fatty acids increased 120% in these cells (Figure 4, D and E). Deletion of APOO 40 N-terminal residues deviated the APOO protein from mitochondria to the cytoplasm and reduced the expression of fatty acid transporters (Figure 4, F and G). Similarly, hearts from APOO-Tg mice displayed a significant increase in fatty acid transporter expression and ACSL expression and activity (Figure 5, A–D). In human atrial appendage samples, *APOO* expression positively correlated with the expression of *CD36*, *FATP4*, and *ACSL3* (Figure 5, E–G). Human heart microarray data mining (see Methods) were in accordance with these results and showed that *CD36* and *FATP2* expression were also increased in the hearts of patients with elevated *APOO* expression (Supplemental Figure 6, A and B). These data suggest that slight *APOO* overexpression affects not only mitochondrial uncoupling and respiration, but also fatty acid metabolism.

APOO increases lipotoxicity. When excessive fatty acid uptake exceeds mitochondrial fatty acid oxidative capacity, toxic lipid storage increases, resulting in lipotoxicity (13). Palmitate treatment of APOO cells induced a dramatic intracellular accumulation of diglycerides and did not significantly affect triglyceride levels compared with control cells. Deletion of the 40 N-terminal aa of APOO significantly reduced cellular diglyceride levels (Figure 6, A and B). Likewise, while triglyceride levels remained the same in controls, diglycerides increased 1.6-fold in APOO-Tg hearts and 2.5-fold in transfected liver (Figure 6, C and D, and Supplemental Figure 4, E and F). In human heart samples, *APOO* mRNA levels correlated with diglyceride levels, but not with triglyceride levels (Figure 6, E and F).

We hypothesized that *APOO* overexpression promotes apoptosis and found positive correlations between mRNA levels of *APOO* and the proapoptotic factor *BAX* in human heart (Figure 7A). Even with modest overexpression of *APOO* in hearts from HFD-fed APOO-Tg mice, *Bax*/*Bcl2* expression ratio and caspase-3 activity were enhanced (Figure 7, B and C). These results were confirmed in vitro with APOO cells, in which increased *Bax* expression and

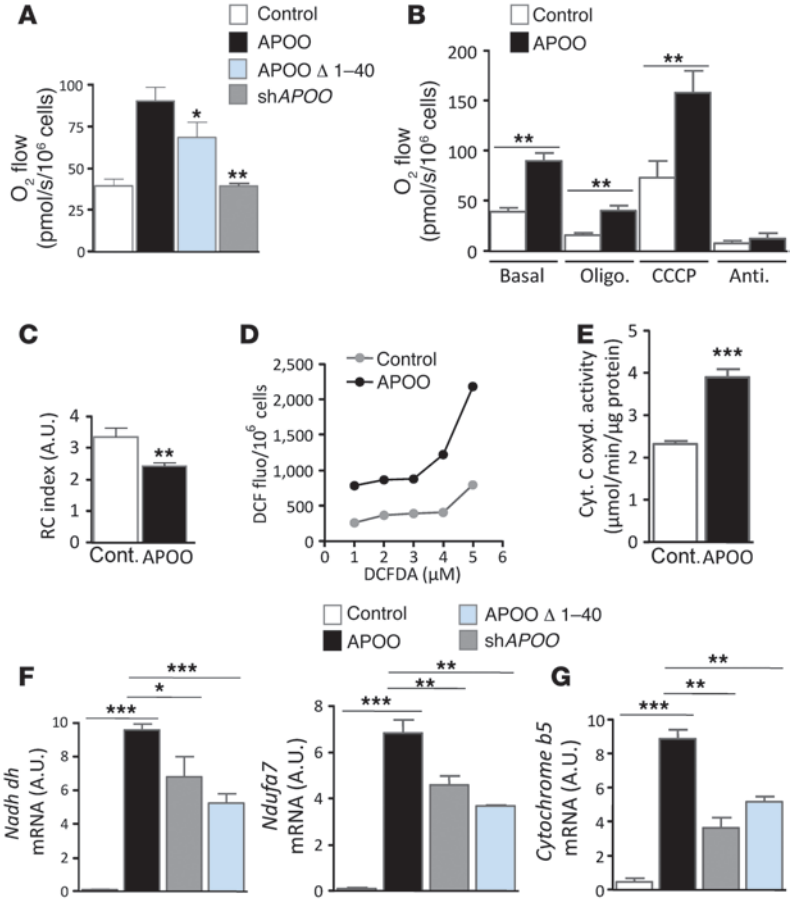

Figure 3

Role of APOO in respiration and oxidative stress in cardiac myoblasts. (**A**) Basal oxygen consumption in control cells, APOO cells, APOO Δ1–40 cells, or APOO cells transfected with sh*APOO* (n = 5). (**B**) Oxygen consumption of control and APOO cells treated with 1.5 μg/ml oligomycin (Oligo), 2 μM carbonyl cyanide m-chlorophenyl hydrazone (CCCP), or 1 μM antimycin (Anti) (n = 5). (**C**) RC index in control and APOO cells. (**D**) ROS, measured in the presence of increasing doses of 2′,7′ dichlorodihydrofluorescein diacetate (DCFDA), in control and APOO cells (n = 4). (**E**) Cytochrome C oxidase activity in control and APOO cells (n = 4). (**F** and **G**) Expression levels of (**F**) mitochondrial complex I and (**G**) mitochondrial complex III genes in control cells, APOO cells, APOO cells subsequently transfected with sh*APOO*, and APOO Δ1–40 cells. (n = 5). *P < 0.05, **P < 0.01, ***P < 0.001. Data represent mean ± SEM.

caspase-3 activity were significantly reversed by sh*APOO* treatment (Figure 7, D and E). This treatment "cured" APOO cells that afterward presented characteristic morphological amelioration, including reduced cell body condensation and cytoplasmic vacuolization. Moreover, *APOO* overexpression dramatically amplified the apoptotic effect of increasing doses of palmitate, which moderately increased caspase-3 activity in control cells (Figure 7F). LCFA uptake exceeds mitochondrial fatty acid oxidative capacity and leads to lipotoxicity, especially in the presence of saturated LCFAs such as palmitate. Excess palmitate generates toxic lipid byproducts, such as diglycerides. This toxicity can be diminished by the addition of unsaturated lipids, such as oleate (14–16), which compels palmitate to produce nontoxic triglycerides. Indeed, APOO cells treated with both palmitate and oleate displayed a 12-fold decrease in diglyceride/triglyceride ratio and a 2-fold decrease in caspase-3 activity (Figure 7, G–I).

These changes should be associated with an increase in expression of PPARα, a transcription factor known to be involved in lipid uptake and β-oxidation (17). Indeed, activity of PPARα was increased in diabetic hearts, and *Ppara* overexpression in mice led to cardiac dysfunction. Expression of *Ppara* was enhanced in APOO cells and in vivo transfected mouse liver (Supplemental Figure 7, A and B). *APOO* expression was also associated with an increase in *PPARA* mRNA levels in human atrial appendage samples and in hearts from APOO-Tg mice (Figure 8, A and B). Accordingly, we found that AMPK was activated in APOO versus control cells (Supplemental Figure 7C).

These results suggest a potential link between pathological *APOO* overexpression and the induction of mitochondrial dysfunction, which should ultimately trigger mitochondrial biogenesis. Expression of *APOO* and PPARγ coactivator 1α (PGC-1α), a master regulator of mitochondrial biogenesis (18), were tightly correlated in human right atrial appendage samples from patients undergoing heart surgery and in hearts from APOO-Tg mice (Figure 8, C and D). The increased mitochondrial synthesis may be an adaptive response that balances the mitochondrial alteration or degradation in autophagosomal vacuoles and multilamellar bodies observed in APOO-Tg hearts and APOO cells (Figure 9, A–D) and attempts to restore falling cellular energy. In support of this, the ATP/AMP ratio was decreased in APOO cells (Supplemental Figure 7D). Ultrastructural analyses have revealed mitochondrial damage in mouse models of the metabolic syndrome and in models of type 1 and type 2 diabetes mellitus. We believe that the pathological overexpression of *APOO* induces a mitochondrial metabolic sink and drives the cell into a vicious cycle that ends in mitochondrial alteration, apoptosis, and cell death in the presence of high extracellular concentration of saturated lipid. This hypothesis could explain the myofibrillar and cardiomyocyte loss observed in APOO-Tg hearts (Supplemental Figure 2C). We propose APOO as a central molecule in lipid and mitochondrial homeostasis.

Discussion

Analysis of numerous human myocardial samples revealed that *APOO* mRNA levels slightly fluctuated between 1 and 5 AU and correlated with mitochondrial dysfunction. Pursuant to this, we were unable to generate cardiac-specific transgenic mice overexpressing *APOO* more than 5-fold, which suggests that *APOO* levels higher than this are extremely deleterious in mouse heart. APOO is thus different from other mitochondrial proteins, like monoamine oxidase A, that can be overexpressed greater than 600-fold in transgenic mouse heart (19). Either *Apoo* gene deletion in yeast (8) or slight overexpressions in mammalian cells (present study) are deleterious for mitochondria. Our results

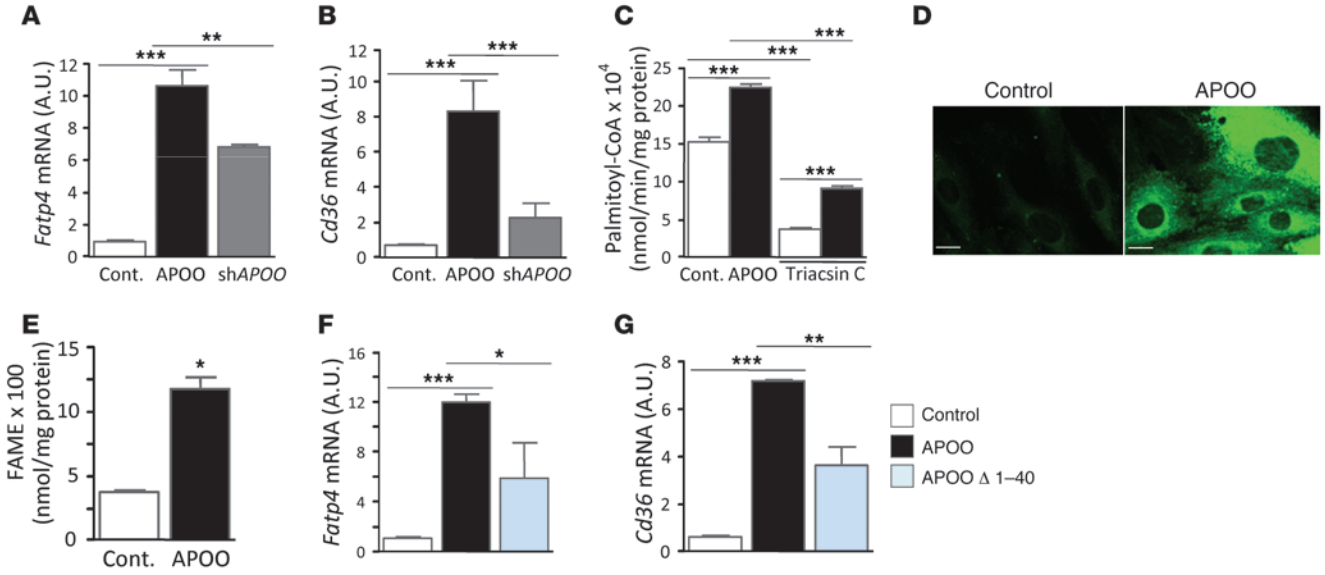

Figure 4
APOO induces fatty acid metabolism in cardiac myoblasts. (**A** and **B**) mRNA expression of (**A**) *Fatp4* and (**B**) *Cd36* in control cells, APOO cells, and APOO cells subsequently transfected with sh*APOO* ($n = 5$). (**C**) Palmitoyl-CoA synthesis rate in control and APOO cells with and without 5 μM triacsin C, an ACSL inhibitor ($n = 5$). (**D**) Confocal microscopy images of control and APOO cells incubated for 2 minutes with BODIPY-palmitate, a fluorescent analog of palmitate. Scale bars: 10 μm. (**E**) Intracellular levels of total fatty acids (fatty acid methyl ester; FAME) in control and APOO cells ($n = 6$). (**F** and **G**) mRNA expression of (**F**) *Fatp4* and (**G**) *Cd36* in control cells, APOO cells, and APOO Δ1–40 cells. *$P < 0.05$, **$P < 0.01$, ***$P < 0.001$. Data represent mean ± SEM.

provided evidence that a basal level of *APOO* expression is needed for optimized mitochondrial function and that tight regulation of *APOO* expression is essential for maintaining normal heart health and homeostasis. In recent studies in yeast (8) and *C. elegans* (9), *Apoo* orthologs have been proposed to be mitochondrial. Interestingly, mutation in the *Apoo* ortholog of *C. elegans* led to cristae disorganization, similar to that observed upon modest *APOO* overexpression in mouse heart. We have previously shown that APOO colocalized with perilipins in cardiac myoblasts (6). This is not in discrepancy with the present work, since perilipins also localize to mitochondria (20).

APOO enhances mitochondrial uncoupling. Consequently, electron transport chain activity and oxygen consumption increase. Previous studies in animal models (21, 22) and in humans (23) suggested that mitochondrial uncoupling plays a key role in the development of cardiomyopathy in obesity and diabetes. However, in *ob/ob* heart studies, mitochondrial uncoupling was not associated with increased protein levels of the

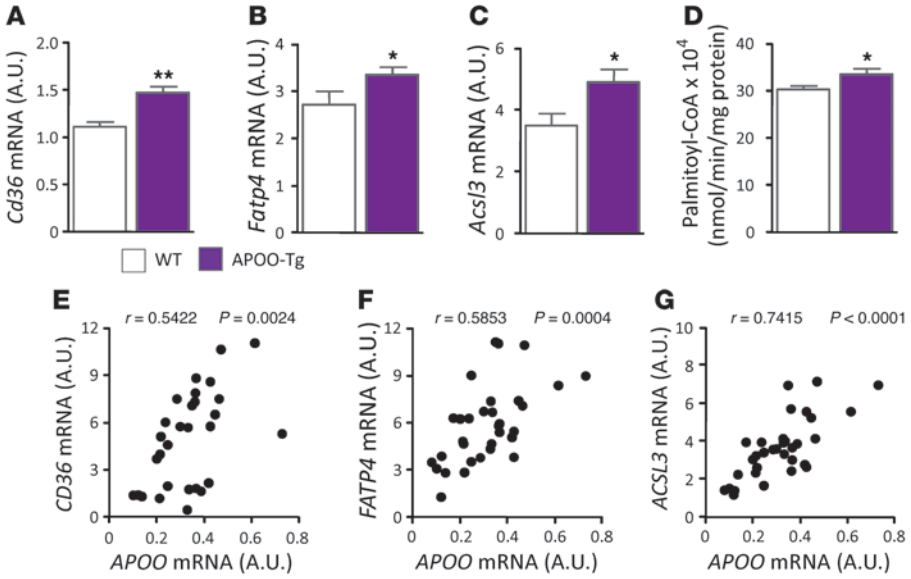

Figure 5
APOO induces fatty acid metabolism in vivo. (**A**–**D**) mRNA expression of (**A**) *Cd36*, (**B**) *Fatp4*, and (**C**) *Acsl3*, as well as (**D**) palmitoyl-CoA synthesis rate, in WT ($n = 11$) and APOO-Tg ($n = 9$) hearts. (**E**–**G**) Correlation between mRNA levels of (**E**) *CD36*, (**F**) *FATP4*, and (**G**) *ACSL3* with *APOO* mRNA in human atrial heart appendage samples ($n = 32$). *$P < 0.05$, **$P < 0.01$. Data represent mean ± SEM

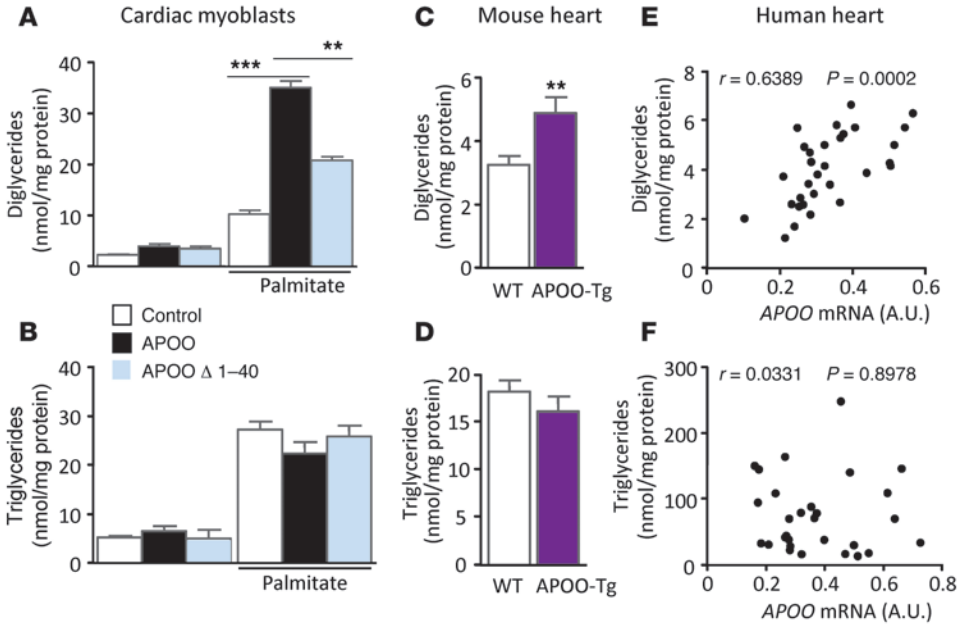

Figure 6
Induction of cardiac lipotoxicity by APOO. (**A** and **B**) Intracellular levels of (**A**) diglycerides and (**B**) triglycerides in control, APOO Δ1–40, and APOO cells with or without 8 hour incubation of 100 μM palmitate (n = 5). (**C** and **D**) Levels of (**C**) diglycerides and (**D**) triglycerides in WT (n = 12) and APOO-Tg (n = 11) mouse hearts. (**E** and **F**) Correlation between *APOO* mRNA level and the intracellular concentration of diglycerides (**E**; n = 30) or triglycerides (**F**; n = 27) in human atrial heart appendage samples. $^{**}P < 0.01$, $^{***}P < 0.001$. Data represent mean ± SEM.

uncoupling proteins (UCPs). Thus, the observed uncoupling in these hearts is independent of changes in the expression of mitochondrial UCPs (24), which suggests the uncoupling may reflect activation of allosteric modification of the UCPs and/or unknown mitochondrial uncoupling mechanisms. Given our present findings, it is tempting to propose that APOO is implicated in this process. In diabetic heart, increased myocardial oxygen consumption is associated with increased fatty acid oxidation in animal models (25, 26) and humans (27). Indeed, obesity and diabetes are forerunners to secondary organ failure through excessive ectopic lipid deposition. This lipotoxicity manifests as cardiomyopathy, myopathy, fatty liver, and diabetes (28). The exact nature of the signal that leads to enhanced and sustained fatty acid uptake in the cardiomyocyte remains uncertain. In cardiomyocytes overexpressing APOO, a specific cascade of events originated with APOO-induced uncoupling. To compensate for the resulting proton leak, the electron transport chain activity increased and depleted the mitochondrial NADH and FADH substrates, generating a mitochondrial metabolic sink. To supplement mitochondria with LCFA, the cardiomyocyte elevated the number of fatty acid transporters. In diabetic heart, fatty acid oxidation and lipid accumulation are considerably increased, and the cardiomyocyte dies by lipoapoptosis (13, 29). The APOO-induced mitochondrial metabolic sink could be an elucidation for the lipid overload. Saturated fatty acids like palmitate exacerbated this toxicity, since more diglycerides are formed. Available data indicate that fatty acid transporters, intracellular fatty acids, and diglycerides have an important role in the etiology of cardiac disease, especially diabetic cardiomyopathy (28, 30–34). In agreement with our present findings, different studies indicate that injury originates inside the myocyte and is not simply secondary to systemic changes associated with hyperlipidemia (35).

Animal lipotoxicity models display evident mitochondrial dysfunction. In these models, lipid accumulation has been proposed to precede the reduction in mitochondrial function. However, converse mechanisms have been proposed in which mitochondrial dysfunction plays a more causative role (36–39). In our models, lipotoxicity appears to be a consequence and not a cause of mitochondrial dysfunction, and our hypothesis implies that mitochondrial failure may be an initial event in diabetic cardiomyopathy.

We also showed that ROS are produced in APOO cells. Several studies have shown that ROS are increased in both type 1 and type 2 diabetes and suggest that increased ROS production is a contributing factor to the development and progression of diabetic cardiomyopathy (40). In support of this, it was reported that overexpression of the mitochondrial antioxidant enzyme manganese superoxide dismutase in the heart of a mouse model of type 1 diabetes mellitus partially reversed altered mitochondrial morphology and function and maintained cardiomyocyte function (41). Moreover, several studies have shown that ROS-mediated mitochondrial biogenesis is likely to occur via the upregulation and actions of PGC-1α. More recently, it was demonstrated that gene expression of *Pgc1a* and its target gene, *Ppara*, are regulated by ROS via several signaling kinases in response to various stimuli, including phosphorylation and activation of AMPK (42). Elevated ROS leads to activation of AMPK, likely via a decline in ATP levels. AMPK activation, in turn, increases mRNA expression of *Ppara* (43–45). *APOO* overexpression reduces ATP levels and activates AMPK, which could explain the high correlation we observed between the expression of *APOO* and that of *PGC1A* and *PPARA* in human and mouse heart. Conversely, AMPK and PPARα can be directly activated by intracellular fatty acids or their derivatives (46). ApoO cells increased intracellular fatty acid levels by 120%. Inhibiting APOO targeting to the mitochondrion or treating APOO cells with sh*APOO* normalized the intracellular levels of fatty acids, which suggests that AMPK and PPARα could be downstream effectors of APOO. The lipid-enhancing effect of APOO is probably achieved by activating cell respiration that results in increasing fatty acid transporter expression, lipotoxicity, and apoptosis.

High or irreversible uncoupling damages mitochondria and contributes to the pathogenesis of a panel of clinically distinct disorders (47). In addition to sustained or irreversible uncou-

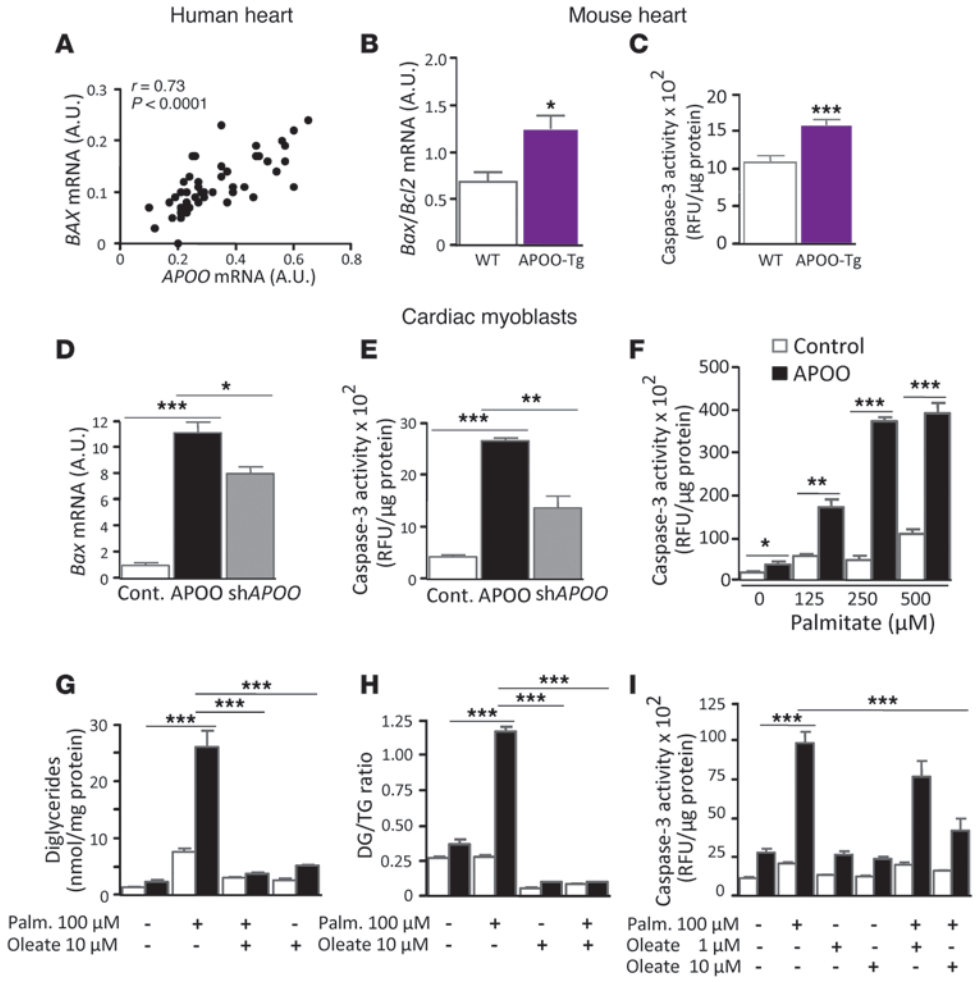

Figure 7
APOO induces apoptosis. (**A**) Positive correlation between *APOO* and *BAX* mRNA levels in human atrial appendage samples (n = 48). (**B** and **C**) *Bax*/*Bcl2* mRNA ratio (**B**) and caspase-3 activity (**C**) in WT (n = 15) and APOO-Tg (n = 16) mouse hearts. (**D** and **E**) *Bax* mRNA levels (**D**) and caspase-3 activity (**E**) in control cells, APOO cells, and APOO cells subsequently transfected with sh*APOO*. (**F**) Activity of caspase-3 in control and APOO-expressing cells incubated overnight with increasing concentrations of palmitate (n = 6). (**G**) Intracellular level of diglycerides in control and APOO cells (n = 4) with or without 12-hour incubation with 100 μM palmitate and/or 10 μM oleate. (**H**) Intracellular diglyceride/triglyceride ratio (DG/TG) in control and APOO cells (n = 4) with or without 12-hour incubation with 100 μM palmitate and/or 10 μM oleate. (**I**) Activity of caspase-3 in control and APOO cells (n = 6) with or without 12-hour incubation with 100 μM palmitate and/or 1 or 10 μM oleate. *P < 0.05, **P < 0.01, ***P < 0.001. Data represent mean ± SEM.

pling, which underlies cell death, it has also been shown that transient and mild uncoupling occurs incessantly in intact cells and in ex vivo beating hearts (48, 49). The baseline or homeostatic function of the uncoupling has been widely studied, and although there is no general agreement, there is a strong conviction that mild uncoupling may be involved in modulating mitochondrial ROS production. Indeed, several studies indicate that physiological levels of ROS are required for the regulation of diverse cellular processes (50–52). Thus, a picture is emerging that uncoupling is a double-edged sword exerting both protective and harmful effects. These findings raise the intriguing possibility that basal APOO level participates in maintaining the inner mitochondrial membrane leak.

In conclusion, we have shown for the first time that APOO induces a rise in respiration, intracellular lipids, and apoptosis. This could be diminished by blocking APOO transfer to the mitochondria or by treating the cells with sh*APOO*. These treatments not only restored the respiration rate, but also reduced fatty acid transporter expression, lipid accumulation, and apoptosis, as indicated by the decreased activity of caspase-3 and expression of fatty acid transporter genes. *Apoo* gene expression is upregulated in heart from animal models after 9 weeks of HFD, i.e., in the early phases of metabolic stress (7). APOO could be a trigger molecule for diabetic cardiomyopathy. Taken together, our findings suggest that partial inhibition of cardiac APOO in individuals predisposed to diabetic cardiomyopathy may represent a valid strategy by which to adjust heart metabolism and protect the myocardium from impaired contractility and function.

Methods

Further information can be found in Supplemental Methods.

Animal studies

Generation of APOO-Tg mice. The *Amhc* promoter–*APOO* transgene was constructed from a 5.5-kb BamHI–SalI fragment containing the murine *Amhc* promoter (53) and a SalI–HindIII cDNA fragment containing the human *APOO* coding sequence (6). The *Amhc* promoter–*APOO* transgene was linearized with NotI, purified by electroelution, concentrated on an elutip-d column (Schleicher and Schuell), and used for nuclear injection in fertilized eggs of B6D2/F1 hybrid females. The microinjected oocytes were then reimplanted in B6CBA/F1 hybrid pseudopregnant foster mothers. 3 transgenic mouse lines were generated and crossed with C57BL/6J mice. Genomic DNA was extracted using DNAeasy blood and tissue kit in a QIAcube apparatus (Qiagen). Offspring were followed by PCR using primers rtiMHCP1F (5′-CCTAGCCCACACCAGAAATGA-3′) and rtiMHCP1R (5′-CCCCACGGACCTCTGAATTA-3′) and Dynazyme II enzyme (Ozyme) as recommended. PCR was performed at least 3 times per mouse, and PCR products were analyzed by acrylamide gel electrophoresis. Animals were

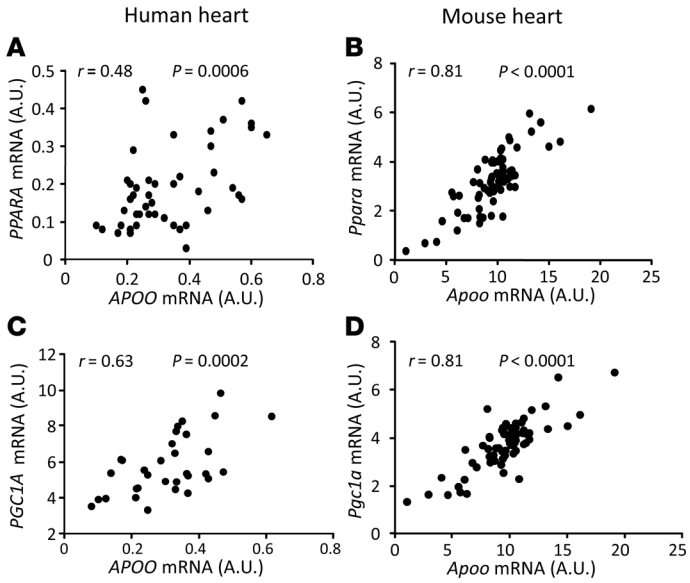

Figure 8
APOO associates with increased PPARα and PGC-1α expression. (**A** and **B**) Correlation between *APOO* and *PPARA* mRNA levels in human atrial heart appendage samples (**A**; $n = 34$) and in hearts from 3 APOO-Tg mouse lines (**B**; $n = 70$). (**C** and **D**) Correlation between *APOO* and *PGC1A* mRNA levels in human atrial heart appendage samples (**C**; $n = 29$) and in APOO-Tg mouse hearts (**D**; $n = 70$).

housed at the Toulouse I2MC animal core facility in a room lit 12 hours per day (6AM–6PM) at an ambient temperature of 22°C ± 1°C.

9- to 10-week old transgenic and nontransgenic littermate male mice were fed a HFD (catalog no. D12492; Research Diet) for 9 weeks.

Cellular models

Cell culture and transfection of H9c2 cardiac myoblasts. H9c2 cells were obtained from the European Collection of Cell Cultures and cultured in DMEM (Life Technologies). Cells were grown in a 5% CO_2 incubator at 37°C with saturating humidity. H9c2 cardiomyoblasts were transfected by electroporation, and pools of transfectants were selected as previously described (54).

Generation of APOO-overexpressing cells. To overexpress human APOO (pTT-APOO), the APOO coding sequence was amplified using primers hAPOO5BamPTT (5′-CGCGGATCCGCACCGAGTTTGCAGTA-3′) and hAPOO3BamPTT (5′-CGCGGATCCTTAGTTCCAGGTGAATTCTTCA-3′) and cloned into the BamH1 site of pTT expression vector (55). To localize APOO in H9c2 cardiac cells, these cells were transfected with pSNAP-APOO vector. pSNAP-APOO was generated by PCR amplification of pTT-APOO using primers SnapApoEcorV-F (5′-AAGATATCATGTTCAAGGTAATTCAGAGG-3′) and SnapApoEcorV-R (5′-TTGATATCCTTAGTTCCAGGTGAATTCTT-3′) and cloned into the EcoRV site of pSNAP-tag (Ozyme). All primers used herein were synthesized by Eurogentec. All restriction enzymes used were from New England Biolabs. All APOO sequences within the expression vectors were verified by DNA double-strand sequencing using ABI PRISM BigDye Terminator version 3.1 Ready reaction cycle sequencing kit (Life Technologies) and loaded on an ABI 3130XL DNA sequencing instrument (Life Technologies).

Knockdown of APOO overexpression. shRNA used to knock down *APOO* gene expression and control shRNA were from MISSION shRNA set (Sh2, TRCN 72707; Sh4, TRCN 72704; Sh5, TRCN 72705; Sigma-Aldrich) and used as recommended by generating pools of stable

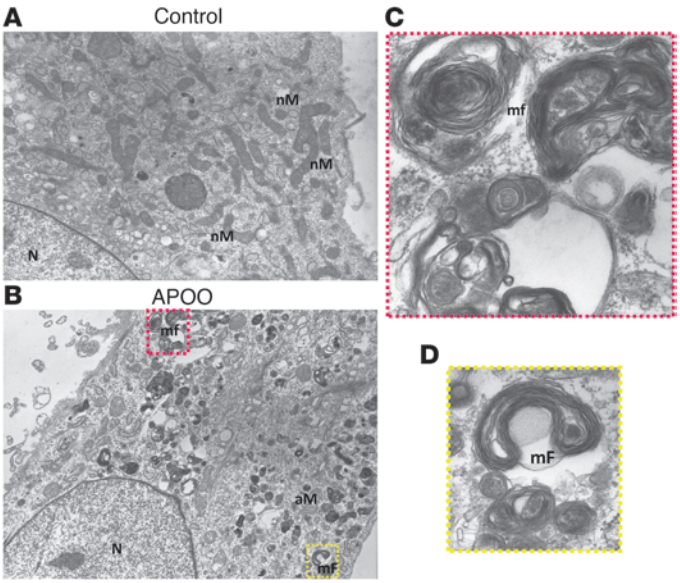

Figure 9
Mitochondrial alteration and degradation in cardiac myoblasts overexpressing APOO. TEM analysis of (**A**) control and (**B**–**D**) APOO cells treated for 24 hours with 100 μM palmitate. Boxed regions in **B** are shown at higher magnification in **C** and **D**. APOO cells demonstrated degradation of mitochondria in autophagosomal vacuoles and multilamellar bodies. mF, myelin figure; N, nucleus. Original magnification, ×6,000 (**A** and **B**); ×50,000 (**C**); ×35,000 (**D**).

transfectants. Empty vector control (no shRNA insert) was also transfected and had no significant effect.

Production and purification of recombinant HIS-tagged APOO. To produce recombinant His6-tagged APOO fusion protein, the *APOO* coding sequence was amplified using primers CherryApoF (5′-GGGAATTC-CATATGTTCAAGGTAATTCAGAGGTCC-3′) and CherryApoR (5′-ATAGTTTAGCGGCCGCCTTAGTTCCAGGTGAATTCTT-3′). The *APOO* fragment was then cloned into the NdeI/NotI sites of pSCodon1.2 (Eurogentec) expression vector. pSCodon1.2-APOO plasmid was then transfected into SE1 *E. coli* cells (Eurogentec). Cells were grown in 2-L Luria-Bertani medium with 50 μg/ml ampicillin (Euromedex) at 37°C with shaking at 200 rpm in an orbital shaker (New Brunswick Scientific) until $A_{600\,nm}$ reached 0.5. Production of recombinant His6-tagged APOO fusion protein was induced by 1 mM isopropyl β-D-thiogalactoside for 3 hours. Cells were pelleted at 5,000 *g* for 15 minutes and frozen in liquid nitrogen. Recombinant APOO was purified using nickel–nitrilotriacetic acid–agarose in batch using an artificial chaperone-assisted refolding method as previously described (6).

Functional genomics

Bioinformatics. Microarray expression data from human heart samples were downloaded from GEO (accession no. GSE1145). This series consisted of 107 myocardial samples collected from patients undergoing cardiac transplantation whose failure arose from different etiologies (e.g., idiopathic dilated cardiomyopathy, ischemic cardiomyopathy, valvular cardiomyopathy, and hypertrophic cardiomyopathy) and from "normal" organ donors whose hearts could not be used for transplants. Arrays were intensity normalized, and hierarchical clustering was applied (average group linkage, Pearson correlation, threshold $r = 0.8$) to identify groups of coexpressed genes. *APOO* expression levels were plotted for the 107 human hearts tested and used to define relevant molecular pathways using both Toppgene (56) and Ingenuity Pathway Analysis (Ingenuity Systems).

Human heart samples

After ethical committee approval, all patients in this study gave written consent for sample collection and molecular analysis prior to inclusion. Patients were carefully selected by physicians from the Department of Cardiology, Toulouse University Hospital, prior to coronary bypass surgery.

Hydrodynamics-based in vivo transfection of the mouse liver

DNA was administered as described previously, with minor modifications, by a single hydrodynamic injection of 50 μg plasmid in 2 ml isotonic NaCl in the tail vein of 20- to 24-g mice over 6–8 s (57).

Echocardiography

Echocardiograms were performed using the Vivid 7 PRO echocardiographic system (GE Medical System) equipped with an i13 L14-MHz linear-array transducer. Images were obtained from chest-shaven rats lightly anesthetized by 1%–2% isoflurane (Baxter) lying on their back with transducers placed on the left hemithorax. 2D parasternal long- and short-axis images of the LV were obtained, and 2D targeted M-mode tracings were recorded at a sweep speed of 200 mm/s. All measurements were performed according to the recommendations of the American Society of Echocardiography. The leading-edge method was applied to 3 consecutive cardiac cycles (n) with the roundness of the LV cavity (2D image) as a criterion that the image was on axis. Great effort was taken to achieve good image quality and to visualize the endocardial and epicardial borders of the heart by gently moving and orientating the transducer. Fractional shortening (a measure of LV systolic function) was calculated as (EDD – ESD)/EDD, where EDD and ESD are end-diastolic and end-systolic diameters, respectively, and expressed as a percentage.

ECG

Surface ECGs were recorded using an ADI system (ADinstruments Ltd.).

Statistics

All results are depicted as mean ± SEM. Multiple comparisons were analyzed by ANOVA — followed, when appropriate, by Dunnett post-hoc test — using Statview 4.5 software (Abacus Concepts). Single comparisons were performed by 2-tailed unpaired Student's *t* test. A *P* value of 0.05 or less was considered significant.

Study approval

All experimental procedures on mice were performed according to INSERM and Genotoul Anexplo animal core facility guidelines for the care and use of laboratory animals. Human heart (right appendage) samples were collected after approval from the "Comité de Protection des Personnes (CPP) Sud Ouest et Outre Mer I et II" (no. DC 2008-452) and informed signed consent of the patients.

Acknowledgments

We thank P. Romanienko for reading the manuscript; A. Galinier for aiding with COX activity measurement; M. Andre, P. Guillou, S. Eddiry, and P. Decaunes for technical assistance; T. Picard for bioinformatics analyses; and the MetaSys and Genotoul networks for electron microscopy, cellular imaging, lipidomics, metabolomics, animal, and biocomputing facilities. This study was supported by INSERM and INSERM/Paul Sabatier University grant.

Received for publication December 9, 2013, and accepted in revised form February 20, 2014.

Address correspondence to: Fatima Smih, INSERM U1048 Equipe no. 7, 1 avenue Jean Poulhés, BP 84225, 31432 Toulouse Cedex 4, France. Phone: 33.5.31.22.41.18; Fax: 33.5.61.32.29.52; E-mail: Fatima.smith-rouet@inserm.fr.

1. Kenchaiah S, et al. Obesity and the risk of heart failure. *N Engl J Med*. 2002;347(5):305–313.
2. Boudina S, Abel ED. Diabetic cardiomyopathy revisited. *Circulation*. 2007;115(25):3213–3223.
3. Mandavia CH, Aroor AR, Demarco VG, Sowers JR. Molecular and metabolic mechanisms of cardiac dysfunction in diabetes. *Life Sci*. 2013;92(11):601–608.
4. Sharma S, et al. Intramyocardial lipid accumulation in the failing human heart resembles the lipotoxic rat heart. *FASEB J*. 2004;18(14):1692–1700.
5. Fein FS. Diabetic cardiomyopathy. *Diabetes Care*. 1990;13(11):1169–1179.
6. Lamant M, et al. ApoO, a novel apolipoprotein, is an original glycoprotein up-regulated by diabetes in human heart. *J Biol Chem*. 2006;281(47):36289–36302.
7. Philip-Couderc P, et al. Cardiac transcriptome analysis in obesity-related hypertension. *Hypertension*. 2003;41(3):414–421.
8. Hoppins S, et al. A mitochondrial-focused genetic interaction map reveals a scaffold-like complex required for inner membrane organization in mitochondria. *J Cell Biol*. 2011;195(2):323–340.
9. Head BP, Zulaika M, Ryazantsev S, van der Bliek AM. A novel mitochondrial outer membrane protein, MOMA-1, that affects cristae morphology in Caenorhabditis elegans. *Mol Biol Cell*. 2011;22(6):831–841.
10. Laffont I, et al. Apolipoprotein E activates Akt pathway in neuro-2a in an isoform-specific manner. *Biochem Biophys Res Commun*. 2002;292(1):83–87.
11. Yang CR, et al. Nuclear clusterin/XIP8, an x-ray-induced Ku70-binding protein that signals cell death. *Proc Natl Acad Sci U S A*. 2000; 97(11):5907–5912.
12. Zhaorigetu S, Yang Z, Toma I, McCaffrey TA, Hu CA. Apolipoprotein L6, induced in atherosclerotic lesions, promotes apoptosis and blocks Beclin 1-dependent autophagy in atherosclerotic cells. *J Biol Chem*. 2011;286(31):27389–27398.
13. Schaffer JE. Lipotoxicity: when tissues overeat. *Curr Opin Lipidol*. 2003;14(3):281–287.
14. Hardy S, El-Assaad W, Przybytkowski E, Joly

E, Prentki M, Langelier Y. Saturated fatty acid-induced apoptosis in MDA-MB-231 breast cancer cells. A role for cardiolipin. *J Biol Chem*. 2003;278(34):31861–31870.
15. Listenberger LL, et al. Triglyceride accumulation protects against fatty acid-induced lipotoxicity. *Proc Natl Acad Sci U S A*. 2003;100(6):3077–3082.
16. Coll T, et al. Oleate reverses palmitate-induced insulin resistance and inflammation in skeletal muscle cells. *J Biol Chem*. 2008;283(17):11107–11116.
17. Finck BN, et al. The cardiac phenotype induced by PPARα overexpression mimics that caused by diabetes mellitus. *J Clin Invest*. 2002;109(1):121–130.
18. Handschin C, Spiegelman BM. Peroxisome proliferator-activated receptor gamma coactivator 1 coactivators, energy homeostasis, and metabolism. *Endocr Rev*. 2006;27(7):728–735.
19. Villeneuve C, et al. p53-PGC-1α pathway mediates oxidative mitochondrial damage and cardiomyocyte necrosis induced by monoamine oxidase-A upregulation: role in chronic left ventricular dysfunction in mice. *Antioxid Redox Signal*. 2013;18(1):5–18.
20. Bosma M, et al. The lipid droplet coat protein perilipin 5 also localizes to muscle mitochondria. *Histochem Cell Biol*. 2011;137(2):205–216.
21. Boudina S, Abel ED. Mitochondrial uncoupling: a key contributor to reduced cardiac efficiency in diabetes. *Physiology (Bethesda)*. 2006;21:250–258.
22. How OJ, Aasum E, Severson DL, Chan WY, Essop MF, Larsen TS. Increased myocardial oxygen consumption reduces cardiac efficiency in diabetic mice. *Diabetes*. 2006;55(2):466–473.
23. Scheuermann-Freestone M, et al. Abnormal cardiac and skeletal muscle energy metabolism in patients with type 2 diabetes. *Circulation*. 2003;107(24):3040–3046.
24. Boudina S, Sena S, O'Neill BT, Tathireddy P, Young ME, Abel ED. Reduced mitochondrial oxidative capacity and increased mitochondrial uncoupling impair myocardial energetics in obesity. *Circulation*. 2005;112(17):2686–2695.
25. Carley AN, Severson DL. Fatty acid metabolism is enhanced in type 2 diabetic hearts. *Biochim Biophys Acta*. 2005;1734(2):112–126.
26. Lopaschuk GD. Abnormal mechanical function in diabetes: relationship to altered myocardial carbohydrate/lipid metabolism. *Coron Artery Dis*. 1996;7(2):116–123.
27. Peterson LR, et al. Effect of obesity and insulin resistance on myocardial substrate metabolism and efficiency in young women. *Circulation*. 2004;109(18):2191–2196.
28. Drosatos K, Schulze PC. Cardiac lipotoxicity: molecular pathways and therapeutic implications. *Curr Heart Fail Rep*. 2013;10(2):109–121.
29. Herrero P, et al. Increased myocardial fatty acid metabolism in patients with type 1 diabetes mellitus. *J Am Coll Cardiol*. 2006;47(3):598–604.
30. Zhou YT, et al. Lipotoxic heart disease in obese rats: implications for human obesity. *Proc Natl Acad Sci U S A*. 2000;97(4):1784–1789.
31. Sparagna GC, Hickson-Bick DL, Buja LM, McMillin JB. Fatty acid-induced apoptosis in neonatal cardiomyocytes: redox signaling. *Antioxid Redox Signal*. 2001;3(1):71–79.
32. Dyntar D, et al. Glucose and palmitic acid induce degeneration of myofibrils and modulate apoptosis in rat adult cardiomyocytes. *Diabetes*. 2001;50(9):2105–2113.
33. Listenberger LL, Schaffer JE. Mechanisms of lipoapoptosis: implications for human heart disease. *Trends Cardiovasc Med*. 2002;12(3):134–138.
34. Chiu HC, et al. Transgenic expression of fatty acid transport protein 1 in the heart causes lipotoxic cardiomyopathy. *Circ Res*. 2005;96(2):225–233.
35. Yagyu H, et al. Lipoprotein lipase (LpL) on the surface of cardiomyocytes increases lipid uptake and produces a cardiomyopathy. *J Clin Invest*. 2003;111(3):419–426.
36. Petersen KF, Dufour S, Befroy D, Garcia R, Shulman GI. Impaired mitochondrial activity in the insulin-resistant offspring of patients with type 2 diabetes. *N Engl J Med*. 2004;350(7):664–671.
37. Graier WF, Malli R, Kostner GM. Mitochondrial protein phosphorylation: instigator or target of lipotoxicity? *Trends Endocrinol Metab*. 2009;20(4):186–193.
38. Patti ME, Corvera S. The role of mitochondria in the pathogenesis of type 2 diabetes. *Endocr Rev*. 2010;31(3):364–395.
39. Schrauwen P, Schrauwen-Hinderling V, Hoeks J, Hesselink MK. Mitochondrial dysfunction and lipotoxicity. *Biochim Biophys Acta*. 2010;1801(3):266–271.
40. Cai L, et al. Attenuation by metallothionein of early cardiac cell death via suppression of mitochondrial oxidative stress results in a prevention of diabetic cardiomyopathy. *J Am Coll Cardiol*. 2006;48(8):1688–1697.
41. Shen X, Zheng S, Metreveli NS, Epstein PN. Protection of cardiac mitochondria by overexpression of MnSOD reduces diabetic cardiomyopathy. *Diabetes*. 2006;55(3):798–805.
42. Irrcher I, Ljubicic V, Hood DA. Interactions between ROS and AMP kinase activity in the regulation of PGC-1alpha transcription in skeletal muscle cells. *Am J Physiol Cell Physiol*. 2009;296(1):C116–C123.
43. Lee WJ, et al. AMPK activation increases fatty acid oxidation in skeletal muscle by activating PPARalpha and PGC-1. *Biochem Biophys Res Commun*. 2006;340(1):291–295.
44. Meng R, et al. AMPK activation enhances PPARalpha activity to inhibit cardiac hypertrophy via ERK1/2 MAPK signaling pathway. *Arch Biochem Biophys*. 2011;511(1–2):1–7.
45. Lee SK, et al. Coenzyme Q10 increases the fatty acid oxidation through AMPK-mediated PPARα induction in 3T3-L1 preadipocytes. *Cell Signal*. 2012;24(12):2329–2336.
46. Grabacka M, Pierzchalska M, Reiss K. Peroxisome proliferator activated receptor alpha ligands as anticancer drugs targeting mitochondrial metabolism. *Curr Pharm Biotechnol*. 2013;14(3):342–356.
47. Andersen JK. Oxidative stress in neurodegeneration: cause or consequence? *Nat Med*. 2004;10(suppl):S18–S25.
48. Petronilli V, et al. Transient and long-lasting openings of the mitochondrial permeability transition pore can be monitored directly in intact cells by changes in mitochondrial calcein fluorescence. *Biophys J*. 1999;76(2):725–734.
49. Wang W, et al. Superoxide flashes in single mitochondria. *Cell*. 2008;134(2):279–290.
50. Zima AV, Blatter LA. Redox regulation of cardiac calcium channels and transporters. *Cardiovasc Res*. 2006;71(2):310–321.
51. Isaeva EV, Shkryl VM, Shirokova N. Mitochondrial redox state and Ca2+ sparks in permeabilized mammalian skeletal muscle. *J Physiol*. 2005;565(pt 3):855–872.
52. Yan Y, et al. Bidirectional regulation of Ca^{2+} sparks by mitochondria-derived reactive oxygen species in cardiac myocytes. *Cardiovasc Res*. 2008;77(2):432–441.
53. Gulick J, Subramaniam A, Neumann J, Robbins J. Isolation and characterization of the mouse cardiac myosin heavy chain genes. *J Biol Chem*. 1991;266(14):9180–9185.
54. Smih F, et al. Transcriptional regulation of adipocyte hormone-sensitive lipase by glucose. *Diabetes*. 2002;51(2):293–300.
55. Durocher Y, Perret S, Kamen A. High-level and high-throughput recombinant protein production by transient transfection of suspension-growing human 293-EBNA1 cells. *Nucleic Acids Res*. 2002;30(2):E9.
56. Chen J, Bardes EE, Aronow BJ, Jegga AG. ToppGene Suite for gene list enrichment analysis and candidate gene prioritization. *Nucleic Acids Res*. 2009;37(Web Server issue):W305–W311.
57. Zhang G, Budker V, Wolff JA. High levels of foreign gene expression in hepatocytes after tail vein injections of naked plasmid DNA. *Hum Gene Ther*. 1999;10(10):1735–1737.